Received: 12 May 2022 | Revised: 10 June 2022 | Accepted: 11 June 2022

DOI: 10.1002/pol.20220266

RESEARCH ARTICLE

JOURNAL OF POLYMER SCIENCE WILEY

Ultra-stretchable, self-healable, and reprocessable ionic conductive hydrogels enabled by dual dynamic networks

Hui Song[1] | **Bing Zhang**[1] | **Qichun Feng**[1] | **Dai Hai Nguyen**[2] | **Chao Zhang**[1] | **Tianxi Liu**[1,3]

[1]State Key Laboratory for Modification of Chemical Fibers and Polymer Materials, College of Materials Science and Engineering, Donghua University, Shanghai, People's Republic of China

[2]Institute of Applied Materials Science, Vietnam Academy of Science and Technology, Ho Chi Minh City, Vietnam

[3]Key Laboratory of Synthetic and Biological Colloids, Ministry of Education, School of Chemical and Material Engineering, Jiangnan University, Wuxi, People's Republic of China

Correspondence

Chao Zhang, State Key Laboratory for Modification of Chemical Fibers and Polymer Materials, College of Materials Science and Engineering, Donghua University, Shanghai 201620, People's Republic of China.
Email: czhang@dhu.edu.cn

Tianxi Liu, Key Laboratory of Synthetic and Biological Colloids, Ministry of Education, School of Chemical and Material Engineering, Jiangnan University, Wuxi 214122, People's Republic of China.
Email: txliu@jiangnan.edu.cn

Funding information

National Natural Science Foundation of China, Grant/Award Numbers: 21875033, 52122303

Abstract

The pursuit of stretchable ionic conductive hydrogels for skin-inspired sensors is highly attractive but challenging due to the difficulty in fabricating an ionic conductive hydrogel with combined characteristics of high stretchability, notch insensitivity, self-healability, and unique reprocessability. Herein, a dual-dynamic-network ionic conductive hydrogel (DICH) with both hydrophobic association network and metal coordination network is one-pot synthesized. Benefiting from the formation of the highly dynamic double networks, the resultant DICH exhibited large stretchability (>2800%) and excellent fracture toughness (4820 kJ m^{-3}). The DICH also demonstrated autonomous healability, notch insensitivity, and unique remoldability because of the formation of the active reversible interactions including hydrophobic association and metal coordination. Due to the integration of high stretchability and favorable ionic conductivity of the DICH containing substantial amounts of electrolytic ions, stretchable ionic strain sensors could be assembled, displaying high sensitivity (gauge factor of 2.6), fast response time (180 ms), and wide response range (0.5%–600% strain). The ionic sensors could also maintain excellent strain-sensing abilities even after being cut/self-healed or reprocessed. Wearable DICH resistive-type strain sensors could be assembled, demonstrating high performance in detecting and distinguishing both large and subtle motions of a human body.

KEYWORDS

dual dynamic network, ionic conductive hydrogels, reprocessability, self-healing performance, wearable strain sensor

1 | INTRODUCTION

Skin-inspired strain sensors are one of the promising wearable sensors that could imitate the sensing functions of human skins by converting physiological signals of joint bending, breathing, and heartbeat into easily processed electrical signals, thus showing the wide-range application in flexible electronics, human-machine interfaces, and soft robotics.[1] The essence of high-performance skin-inspired strain sensors is to construct ultra-stretchable conductors that are sensitive to external strains. Currently, the most reported stretchable conductors have been fabricated by the compounding of intrinsically conductive components like carbon nanomaterials, metal nanoparticles, and conducting

polymers with elastic polymer matrices.[2] However, conventional fabrications of these stretchable conductors are complicated and tedious, making them difficult to be manufactured on a large scale.[3] Meanwhile, the stretchability of these stretchable conductors is mainly determined by the tensile limits of elastic polymer matrices, and irreversible damages of rigid conductive components under large strains severely limit their application in adapting to complex deformations for wearable skin-inspired strain sensors.[4] Therefore, multifunctional stretchable conductors with the integrated features of easy fabrication, structural stability and high stretchability are largely demanded in developing the next-generation skin-inspired strain sensors.

Ionic conductive hydrogels are one kind of hydrogel materials that could realize the conductivity by carrier transferring through the directional movements of free ions.[5] Due to their biocompatibility and tailored mechanical flexibility, ionic conductive hydrogels demonstrate great potential as stretchable conductors for skin-inspired strain sensors.[6] However, conventional ionic conductive hydrogels that are composed of a single network (SN) have relatively weak mechanical moduli, resulting in mismatching of mechanical properties with human skin as well as poor wearability.[7] The construction of ionic conductive hydrogels with rigid/ductile double networks (DN) provides an effective route for developing hydrogels with excellent mechanical properties.[8] Under large deformations, the destruction of the rigid network in the DN hydrogels could efficiently dissipate the fracture energy and thus greatly raise the apparent work required to rupture the material.[9] However, fractures of the rigid network tend to cause irreversible destructions of DN hydrogels, leading to severe safety problems and resource wastes.[10] The DN hydrogels usually exhibit unsatisfying self-healing performance, and their relatively low healing efficiency is often realized by applying the external stimuli of heating and UV lighting.[11] Besides, fabrications of DN hydrogels involve the immersion of SN hydrogels into a monomer solution of the second network for secondary polymerization, which is rather complicated and time-consuming. The two-step fabrication process also leads to the formation of uneven network structures, which make the DN hydrogels prone to form stress concentrations during the deformation.[12] More importantly, once the DN hydrogels have been formed, it is difficult to achieve reprocessability due to the existence of the permanent cross-linked structures, which greatly restricts the reuse of hydrogels on surfaces of complex objects and leads to resource wastes.[13] Therefore, the development of DN ionic conductive hydrogels with high mechanical strength, autonomous healability and reprocessibility is critical yet challenging.

Herein, a dual-dynamic-network ionic conductive hydrogel (DICH) has been one-pot fabricated, which consists of highly interplayed dynamic networks, including the hydrophobic association network and metal coordinated network. The hydrophobic association network (P[AA-co-OMA]) is formed by random copolymerization of acrylic acid and octadecyl methacrylate, while the metal coordinated network (Ca-XG) is obtained by the xanthan gum chains coordinated by calcium ions. The highly dynamic dual-network imbues the resultant DICH with moderate mechanical strength (0.27 MPa), large elongation at break (>2800%), and high fracture toughness (4820 kJ m^{-3}). The dynamic hydrophobic association and metal coordination among the DICH could efficiently dissipate the fracture energies through their reversible fracture and recombination, endowing the hydrogels with high notch insensitivity, remolding, and self-healing with a high healing efficiency of >95%. Benefiting from their high stretchability and large ionic conductivity, the DICH is presented as a stretchable ionic conductor to construct a resistive strain sensor, exhibiting stable sensing signals over a wide strain range (0.5%–600%) and fast response to strain (180 ms). A proof-of-concept wearable ionic sensor is therefore constructed, realizing the real-time monitoring of complex human movements of swallowing, finger, elbow, and knee bending. Importantly, the sensor could maintain normal operations after being cut and self-healed or remolded for reprecessibility. This study thus provides new ideas for developing ultra-stretchable ionic conductive hydrogels with highly dynamic reversibility for the next-generation skin-inspired sensors.

2 | RESULTS AND DISCUSSION

The design principle for the construction of the ultra-stretchable ionic conductive hydrogels is to introduce unique dual dynamic networks that are composed of hydrophobic association network and metal coordinated network (Figure 1). Natural polysaccharides are typical multifunctional polymeric materials with excellent biocompatibility and biodegradability. Therefore, the preparation of the DICH using the XG as the precursor to form the metal coordinated network has unique advantages. First, the XG as a natural anionic polysaccharide polymer is prone to form strong coordination interactions with various metal cations (Ca^{2+}, Pb^{2+}, Al^{3+}, etc.), facilitating the construction of ionic conductive hydrogels with adjustable coordination strengths.[14] Second, the XG has good stability in an acidic solution, which is beneficial for preparing acidic hydrogels like the conventional poly (acrylic acid) (PAA) hydrogels. Third, the XG is composed of a *D*-glucose backbone chain linked by β-1,4 glycosidic bonds and trisaccharide side chains,[15] which

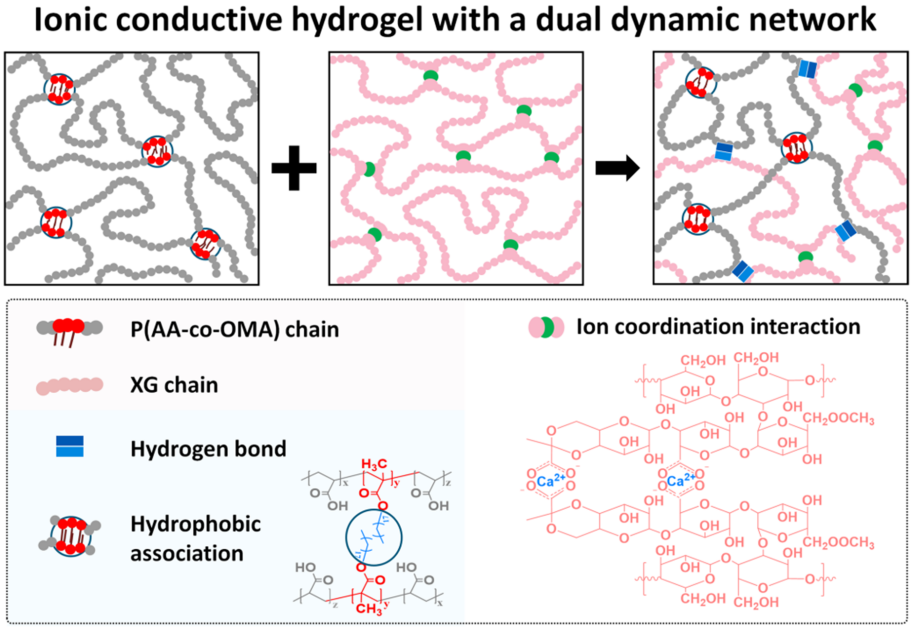

FIGURE 1 Schematic illustration of the design of DICH with dual dynamic networks

therefore exhibits a high molecular weight with a long-chain backbone, which helps to enhance the mechanical strengths of hydrogels by increasing the entanglement degrees between individual molecular chains.[16] Finally, the abundant hydroxyl and carboxyl groups on the galactose ring in the XG provide abundant binding sites for the formation of strong intramolecular and intermolecular noncovalent bonds, thus forming strong hydrogel network structures.[2b] The DICH was fabricated by a one-pot free-radical polymerization. All the reactants of XG, $CaCl_2$, AA monomers, OMA and thermal initiator were dissolved in the SDS/NaCl aqueous solution, followed by thermal-initiated in situ polymerization. There are two types of active dynamic networks in the DICH. One is formed by the metal coordination interactions between the divalent cation and the carboxyl groups in XG (Ca-XG). The other is the copolymerization of the hydrophobic monomer OMA with the hydrophilic monomer AA in the presence of the SDS micellar solution to form a poly(acrylic acid-co-octadecyl methacrylate) (P[AA-co-OMA]) hydrophobic association network. Moreover, dense hydrogen bonds also exist between the two networks of Ca-XG and P(AA-co-OMA). In the DICH system, the Na^+ and Cl^- ions used in the preparation process and the H^+ ions that are ionized from the XG chains could act as the charge carriers to provide the conductivity.

As indicated by scanning electron microscope (SEM) images, the lyophilized hydrogels maintain interconnected three-dimensional porous structures. Porous structures are irregularly distributed among the freeze-dried P(AA-co-OMA) hydrogels due to the formation of SDS micelles (Figure 2A). These micelles serve as the crosslinking points to form the P(AA-co-OMA) crosslinked networks, suggesting the formation of hydrophobic associations. The pore structures of the resulting DICH are dramatically affected by the concentrations of XG. When the concentration of XG increases from 5 to 15 mg mL^{-1}, the crosslinking density of DICH increases significantly, and the pore distribution becomes uniform due to the formation of the Ca-XG networks and the dense hydrogen bonds between the dual dynamic networks (Figure 2B–D).

Fourier transform infrared (FTIR) spectra were used to demonstrate the presence of the dual dynamic networks, whose formation is crucial to the comprehensive properties of DICH. The broad characteristic peak at 3425 cm^{-1} in the XG belongs to the stretching vibration of the hydroxyl groups, while the absorption peaks at 1726 and 1619 cm^{-1} are assigned to the stretching modes of C═O in the acetyl groups and the asymmetrical stretching vibration of C═O in pyruvate groups,[17] respectively (Figure 2E). Compared with the XG, the peak at 3425 cm^{-1} moves to 3434 cm^{-1} in the Ca-XG hydrogels, proving the formation of hydrogen bonds among the Ca-XG chains. The absorption peak at 1726 cm^{-1} shifts to 1720 cm^{-1}, while the absorption peak at 1619 cm^{-1} shifts to 1631 cm^{-1}, revealing that the coordinating interactions of COO^- and Ca^{2+} have occurred.[14,18] Both P(AA-co-OMA) and DICH-2 exhibit the characteristic absorption peaks at 2920 and 2851 cm^{-1} (Figure 2F), which are due to the stretching vibrations of methylene groups in the OMA, indicating that the P(AA-co-OMA) hydrophobic association network was formed by the copolymerization of AA and OMA.[16] Compared with the P(AA-co-OMA) hydrogel, the wide peak assigned to the -OH stretching

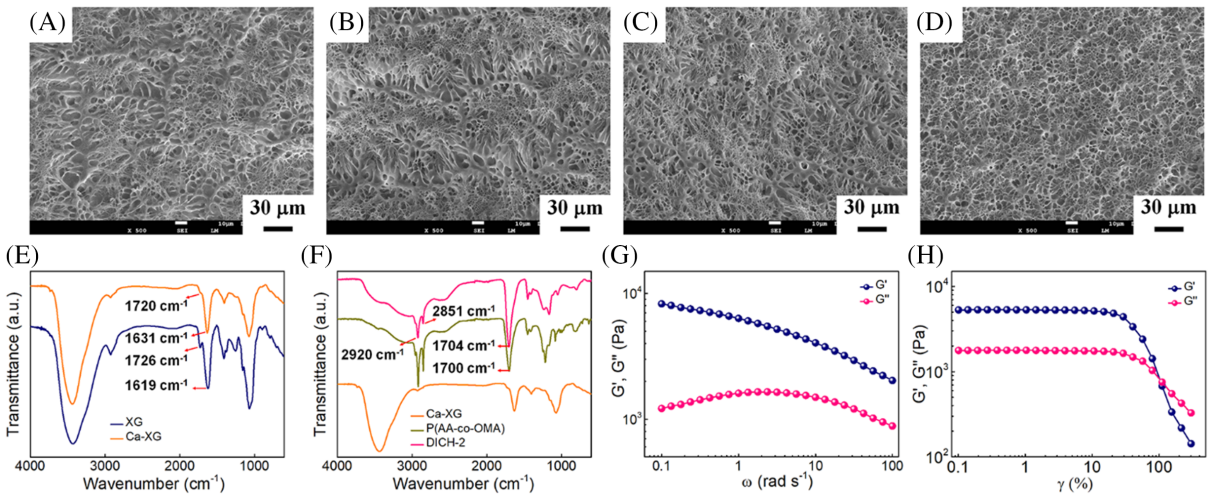

FIGURE 2 Structural characterizations of DICHs. SEM images of freeze-dried samples of (A) P(AA-co-OMA), (B) DICH-1, (C) DICH-2, and (D) DICH-3. (E) FTIR spectra of XG and Ca-XG hydrogel. (F) FTIR spectra of Ca-XG, P(AA-co-OMA), and DICH-2. (G) Oscillatory frequency sweep measurement at a shear strain of 0.5% and (H) oscillatory amplitude sweep measurement at an angular frequency of 2 rad s^{-1} for DICH-2

vibration at about 3438 cm^{-1} in the DICH-2 is more obvious, which is caused by the formation of Ca-XG metal coordination networks. Compared with the characteristic peaks of P(AA-co-OMA) and Ca-XG hydrogel, no new absorption peaks appear in DICH-2, indicating that no new chemical bonds are formed between the two dynamic networks.[19] The characteristic peak of P(AA-co-OMA) at 1700 cm^{-1} belongs to the stretching vibration of C═O groups, which slightly shifts to a relatively high frequency at 1704 cm^{-1} in the DICH-2 due to the formation of intermolecular hydrogen bonds between the Ca-XG and P(AA-co-OMA) networks.[20]

To demystify the dynamic mechanical properties of DICH, we measured the rheological properties of G' and G'' at various frequencies under a constant strain (Figure 2G). The G' decreases, while the G'' increases to a maximum value and decreases as the frequency rises, which is attributed to the change of crosslinking density caused by the dissociation and subsequent formation of the dynamic reversible interactions.[21] The G' exceeds the G'' within the frequency range of 0.1–100 rad s^{-1}, reflecting the solid-like nature of the DICH-2.[22] The linear viscoelastic region of DICH-2 was determined by an oscillatory amplitude sweeping test (Figure 2H). The G' is larger than the G'' at a small shear strain (<20%, like an elastic solid), and the G' is crisscrossed with the G'' at the oscillatory strain amplitude of 110%, revealing the collapse of the DICH-2 network.[23] The break of noncovalent bonds transforms the DICH-2 of a solid elastic network into a viscous fluid.

Benefiting from the simplicity and availability of the one-pot in situ polymerization methodology, the DICHs could readily and precisely be adapted to various shapes, such as a heart, a flower, a triangle, and a star (Figure 3A), showing high designability. Besides, the DICHs exhibit high mechanical strength due to the presence of the coordination with metal ions, the dual dynamic networks and the dense hydrogen bonds. The obtained DICHs are tough and capable of withstanding different deformation modes, such as compression (Figure 3B) and elongation (Figure 3C), while without any visible damage. The DICHs could recover to their original dimensions with negligible residue strains upon removing deformation forces, demonstrating their shape-recovery characteristics.

To characterize the effects of the dual dynamic networks on the mechanical properties of DICH, the uniaxial tensile tests of P(AA-co-OMA), XG/P(AA-co-OMA) and DICH-2 were measured and compared. The Ca-XG hydrogel was not tested by mechanical tests because it is not self-supporting (Figure S2). Therefore, the Ca-XG hydrogel does not have mechanical strength and elongation at break. The P(AA-co-OMA) hydrogel displays an extremely low tensile strength of 33 kPa (Figure 3D). In contrast, the XG/P(AA-co-OMA) hydrogel that is prepared without the addition of $CaCl_2$ possesses a moderate tensile strength of 168 kPa due to the formation of hydrogen bonds between the P(AA-co-OMA) and XG chains, which thus increases the crosslinking density of hydrogels (Figure S3). The tensile strength of DICH-2 reaches up to 270 kPa, while the fracture strain is up to 2800% (Figure S4). The significant improvement in mechanical strength is ascribed to the formation of the dense hydrogen bonds between the Ca-XG metal coordination networks and P(AA-co-OMA) hydrophobic association

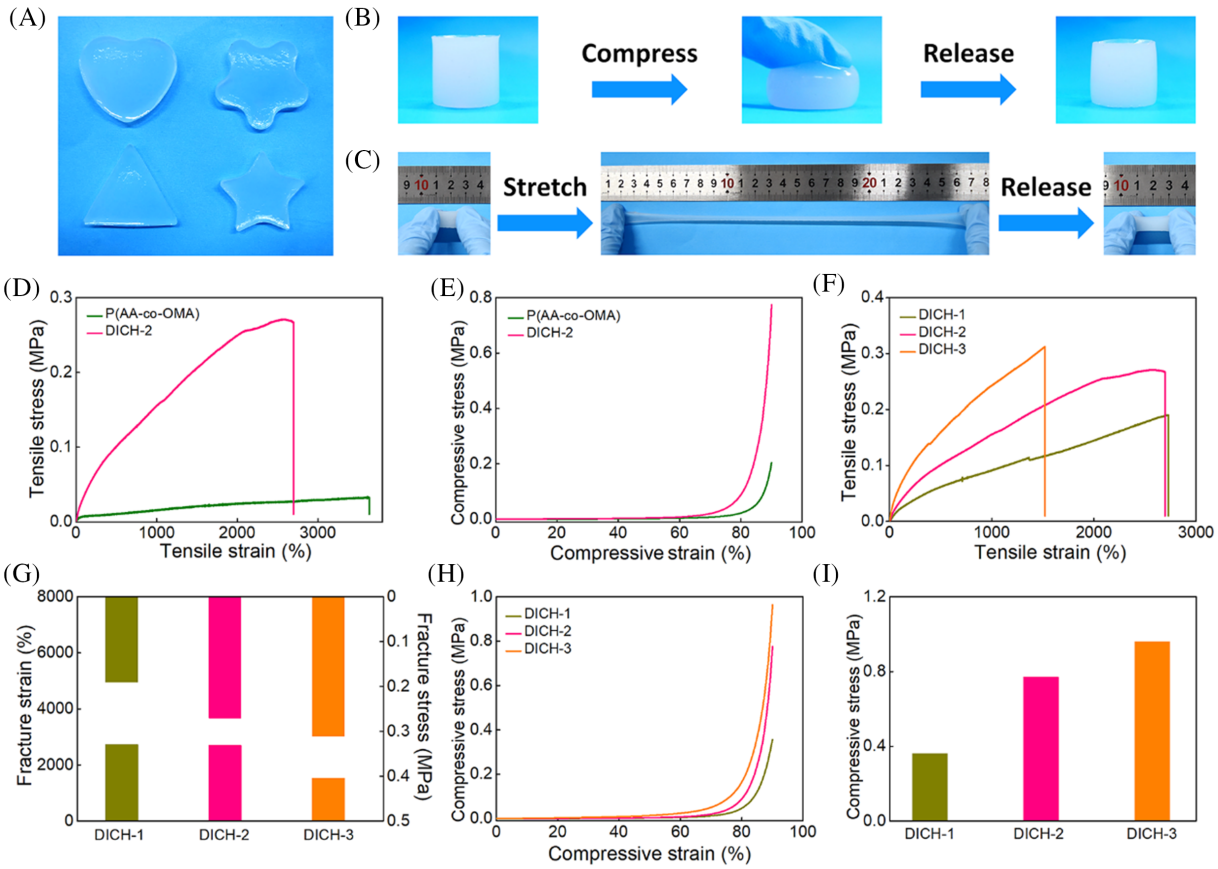

FIGURE 3 Mechanical properties of DICHs. (A) Optical images of DICH-2 in diverse shapes. Optical images of DICH-2 under (B) compressing/releasing and (C) stretching/releasing processes. (D) Tensile stress–strain curves and (E) compressive stress–strain curves of P(AA-co-OMA) and DICH-2. (F) Tensile stress–strain curves, (G) fracture strain and fracture stress, (H) compressive stress–strain curves, and (I) compression stress of various DICHs

networks. Moreover, the coordination with metal ions also contributes to the improvement of tensile strength.[24] The sharp increase in the mechanical strength of DICH-2 also proves the successful construction of the dual dynamic network.[25] In the compressive measurements, the maximum compression strength of DICH-2 at 90% strain is 770 kPa, which is 3.9 times of P(AA-co-OMA) hydrogels (200 kPa) (Figure 3E). Therefore, dual dynamic networks are indispensable to improve the mechanical strength and toughness of DICH.

A series of tensile and compressive experiments were conducted to quantitatively assess the mechanical properties of DICHs in response to XG concentrations. The DICH-1, DICH-2, and DICH-3 represent the as-obtained hydrogels with the XG concentration at 5, 10, and 15 mg mL^{-1}, respectively. Obviously, with the increase of the initial XG concentration, the tensile stress increases from 190 to 310 kPa, whereas the elongation at break decreases monotonously from 2726% to 1520% (Figure 3F, G). The toughness of DICH increases first and then decreases, and exhibits a maximum value of 4820 kJ m^{-3} (Figure S5). The soft material toughens under the massive XG loadings due to the network densification by forming Ca-XG networks and dense hydrogen bonds. Taking into the tradeoff between stress and strain, the DICH-2 is selected for the subsequent investigations. Successive stretching-releasing tests were performed to assess the energy dissipation mechanism. As the maximum strain increases from 50% to 600%, more extensive crosslinked networks are broken to dissipate energy, leading to a significant increase in hysteresis loops (Figure S6a). Under the 300% strain, the hysteresis loop recovery is not obvious with the increase in interval time, indicating that the fracture energy is dissipated by the reversible breaking of noncovalent bonds (Figure S6b). The compression measurements show that the increased XG concentration improves the compressive strength (Figure 3H,I). The maximum compressive strength of DICH-3 is 960 kPa at 90% deformation, indicating that the hydrogel is resistant to compressive forces. Cyclic compressing-recovering tests were performed on the same hydrogel samples at the maximum strain range of 10%–80% (Figure S7a). The hysteresis loop of DICH-2

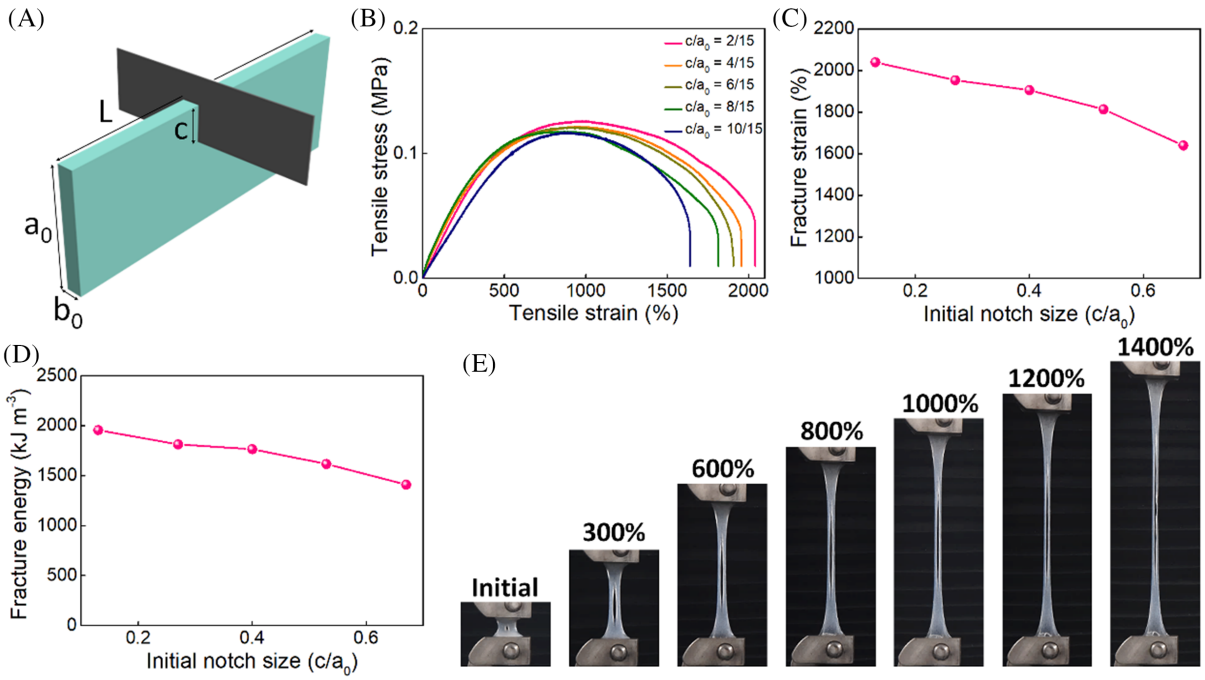

FIGURE 4 Notch insensitivity performance of DICHs. (A) Schematic diagram of a notched DICH-2. (B) Tensile stress–strain curves, (C) fracture strain, and (D) fracture energy of DICH-2 with various crack lengths. (E) Optical images of DICH-2 with a central notch stretched to different strains

increases with increasing the maximum strain. At the compressive strain of 50%, the hysteresis loop is difficult to recover with the increase in interval time (Figure S7b), which lays the foundation for the remolding feature of DICH.

The existence of active dynamic reversible interactions of energy dissipating provides the DICH with strong resistances to external damage, which is significantly required in practical applications. That is to say, when the DICH with a notch is stretched, the notch is relatively insensitive, which makes the DICH less likely to break at the notch. DICH-2 samples with various initial notch sizes were stretched by tensile measurement (Figure 4A,B). Interestingly, the different notch lengths lead to different fracture degrees of the specimens under stress. Both yielding and necking phenomena are observed in our notched DICH-2. When the samples are stretched, the notch does not expand immediately. Although the stress continues to act on the incision, these dynamic expanded networks effectively dissipate energy, thus reducing the stress concentration at the notch.[26] Furthermore, the fracture strain and fracture energy of DICH-2 were calculated by stress–strain curves (Figure 4C,D). Even though notch length such as 10 mm is introduced to the DICH-2 sample, it continues to operate to a 1640% strain because of its exceptional toughness, which prevents damage evolutions under stretching. The fracture energy maintains over 1900 kJ m^{-3}, proving that DICH has notch insensitivity and is not easy to fracture in practical applications.

After stretching one central notched DICH-2, the notch narrows and lengthens instead of expanding to the periphery. The notched DICH-2 continues to operate to 1400% strain (Figure 4E), indicating the excellent crack resistance of the material. The excellent notch-insensitivity ability of DICH-2 originates from physical crosslinking through the active dynamic bonds, including metal coordination, hydrophobic associations and hydrogen bonds. When the notched DICH-2 is stretched, the P(AA-co-OMA) network dissipates energy near the notch and transfers tensile stress to large adjacent regions. At the same time, the Ca-XG network bridges the cracks and stabilizes the deformation, thus avoiding the stress concentration and inhibiting crack propagation. Thus, our hydrogels have superior crack resistances to constant mechanical damage without interrupting their operation.

Self-healing performance without external stimulation endows ionic conductive hydrogels with advanced abilities to suffer damage in practical applications.[27] The gel systems based on hydrophobic associations, metal coordination and hydrogen bond interactions exhibit excellent self-healing properties at room temperature without additional stimulation.[28] Benefiting from the large amounts of reversible dynamic noncovalent bonds mentioned above, the resulting DICH also shows excellent self-healing performance

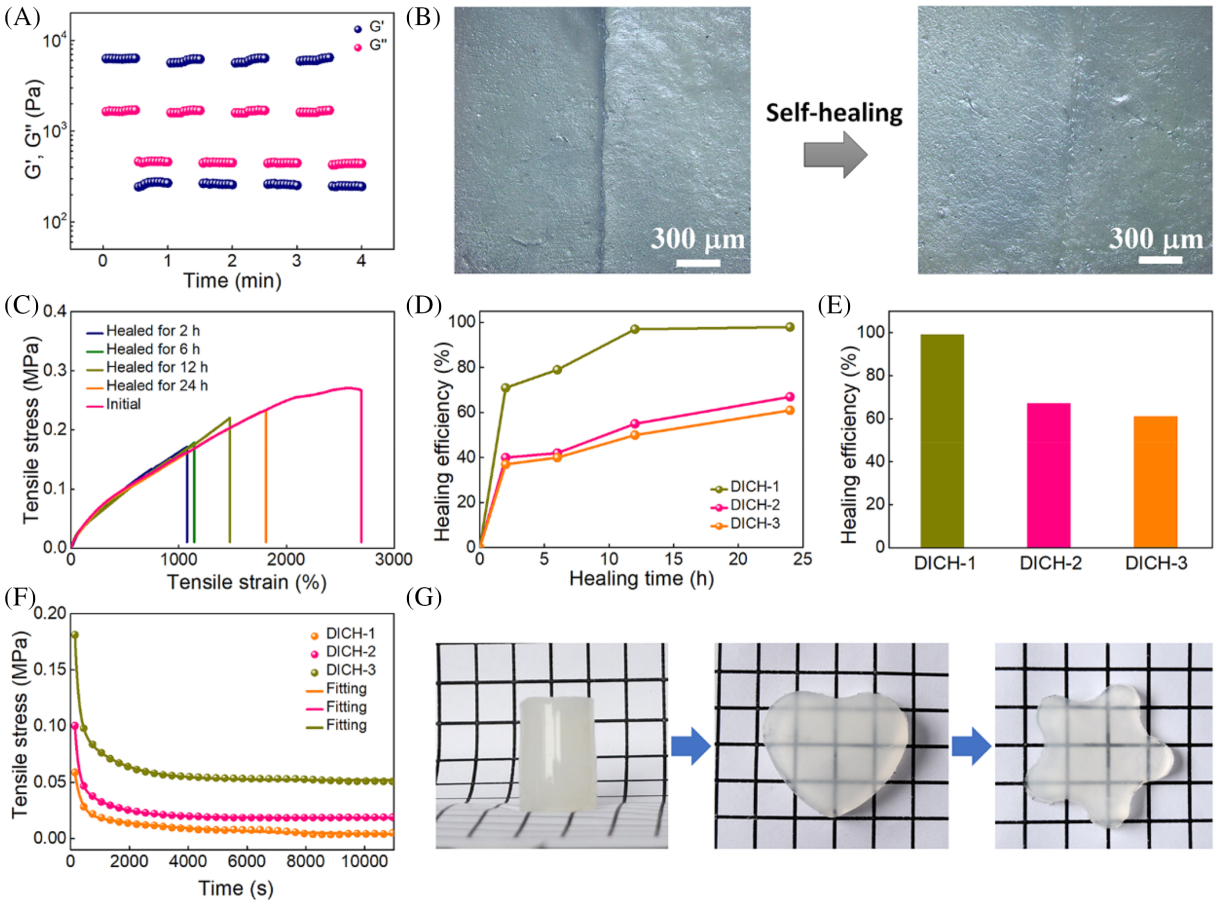

FIGURE 5 Self-healing and reprocessing performance of DICHs. (A) Alternate step strain sweep tests with alternating shear strains of 1% and 150% with 30 s for DICH-2. (B) Optical microscope images of a DICH-2 before and after self-healing. (C) Tensile stress–strain curves of the original and healed DICH-2 after different healing times. (D) Healing efficiency of DICHs after different healing times. (E) Healing efficiency of DICHs after healing for 24 h. (F) Stress relaxation curves of DICHs. (G) the reprocessing capability of DICH-2: The original sample (left), the sample after remolding (middle and right)

without any outer stimuli or healing agents. To determine the self-healing performance of DICH after the failure under high strain, continuous strain sweep tests consisting of an alternate small oscillating force and a large one at a constant angular frequency were developed (Figure 5A). Initially, the G' is constantly ~6250 Pa and always higher than that of G'' (1650 Pa), proving that the DICH-2 network is conserved adequately. Subsequently, the DICH-2 is treated with a high shear strain of 150%. The G' and G'' decrease dramatically, and the G'' is larger than G', implying that the network of DICH-2 is interrupted under the high strain. Subsequently, when the strain amplitude is returned to 1%, the G' returns to its original value instantaneously and is higher than G'', proving the effective recovery and excellent self-healing capability of DICH-2 after the damage.[29] The disruption-recovery process could be repeated several times without deteriorating the mechanical properties of DICH-2. This unique performance is attributed to the inherent reversibility of hydrophobic interactions, metal coordination and hydrogen bonds between P(AA-co-OMA) and Ca-XG dual networks.

Digital images show that no cracks are observed at the contact interface of the DICHs after healing for 24 h, and the healing hydrogel could be stretched to several folds of its original length without fractures (Figure S8). The DICH-2 could entirely self-heal the crack, indicating its highly effective self-healing properties (Figure 5B). To quantitatively assess the self-healing ability, uniaxial tensile experiments on the healed DICHs compared to the original hydrogels (Figures 5C and S9). The tensile stress and strain of healed DICH could be significantly enhanced by prolonging the healing time. Self-healing efficiency (*HE*) is the ratio of restored toughness to the original toughness, which considers the recovery of both tensile strain and stress. The *HE* increases with the increasing self-healing time due to increased chain mobilities among the DICH for a long time (Figure 5D).[30] Notably, the *HE* of DICH remains above 95% at an XG

concentration of 5 mg ml^{-1}, while the *HE* decreases to 61% when the concentration of XG increases to 15 mg ml^{-1} (Figure 5E). The excessive XG results in a significant increase in the crosslinking density, which weakens the diffusion capacity of micelles and ions as well as limits the newly generated interactions between polymer chains, leading to a sharp decline in *HE*.[31] To further illustrate the self-healing performance of DICH after multiple cutting and self-healing cycles, the cut and self-healed DICH-2 was further tested (Figure S10). The self-healing takes place even after the fifth destruction, further indicating the excellent self-healing ability of the DICH.

More than the recovery in mechanical properties, the electrical properties such as ionic conductivity are also completely restored. The resistance varies from a steady-state to infinity when the DICH-2 sample is cut into two halves and returns to its initial value after a decrease caused by a slight pressure during the cutting and self-healing processes (Figure S11), indicating the complete reconstruction of conductive channels. A battery-powered circuit consisting of a LED with a piece of DICH-2 as the conductor was further constructed to demonstrate the restored conductivity (Figure S12). The LED light goes out in an open circuit due to the cleavage of DICH-2. Once the two separate hydrogels self-heal together, the conductive pathway is restored, and the LED bulb is turned on again. Owing to the inherent tensile performance and self-healing properties, the LED still glows after the healed DICH-2 is stretched, reflecting the efficient recovery of ionic conductivity.

After DICH samples are cut in half, the hydrophobic associations, metal coordination and hydrogen bonds on the cut surfaces are destroyed. When the fresh surfaces of the cut hydrogels come into contact, the outermost DICH chains tend to be recombined with SDS micelles on the interface through hydrophobic interactions. In addition, Ca^{2+} ions synchronously chelate with carboxyl groups distributed on XG chains, forming a robust "dynamic zipper" that improves the self-healing ability. Hydrogen bonds between the hydroxyl groups of XG and the carboxyl groups on the P(AA-co-OMA) chain further contribute to the self-healing properties. Taken together, the introduction of such self-healing properties makes DICH has great potential in the application of self-healable wearable devices.

The reprocessing ability enables the hydrogel to change its original shape according to the actual application requirements, effectively avoiding the waste of materials. The DICH crosslinked by dynamic reversible interactions has a good secondary processing capacity. According to the stress relaxation curves, the tensile stress decreases rapidly and then tends to desmonstate a nonzero value (Figure 5F). The stress is related to the chain segment orientation and the breaking/reforming kinetics of noncovalent bonds. During the stretching, the abundant noncovalent bonds carry a significant amount of stress, which induces the chain segment orientation. During the relaxation, the noncovalent bonds could break and the oriented chain segments are instantaneously relaxed, resulting in a stress reduction. Although these chains might reattach by the formation of reversible noncovalent bonds, the reconnected chains are in their relaxed states and could carry no tensile energy that does not contribute to chain segment orientation and stress improvement.[32] This explains the relaxation of stress during the strain holding. We use the generalized Maxwell function to fit the stress relaxation curves:

$$\sigma(t) = A_1 e^{(-t/\tau_1)} + A_2 e^{(-t/\tau_2)} + \sigma_{re},$$

where $\sigma(t)$ is the relaxation stress, τ_1 and τ_2 are the relaxation time, A_1 and A_2 are the pre-exponential factors, and σ_{re} is the stress at equilibrium. Although the different DICH samples exhibit various degrees of relaxation, all the relaxation dynamics could be well fitted by the Maxwell function. The DICH-3 has maximum stress values of equilibrium state and maximum relaxation time because the distance between the crosslinking points in the DICH crosslinked network decrease with the increase of XG contents. It becomes more difficult for the long polymer chains between the crosslinking points to eliminate stress by tailoring the molecular conformation.[13]

The glass transition temperature (T_g) of PAA is approaching 100 °C.[33] With the copolymerization of OMA and formation of Ca-XG networks, the density of physical crosslinking points including the hydrophobic association, the metal coordination and the hydrogen bonds increase, which deteriorates the chain mobility, thus increasing the T_g of DICH to more than 100 °C.[34] The temperature closer to the T_g is more conducive to the movements of molecular chains, resulting in the stress relaxation. Therefore, cylindrical samples were pressed into a "heart" or "flower" mold at a high temperature of 70 °C for remolding and then taken out to observe their deformation. The deformation gradually tends to be irreversible with the extension of time. Finally, it exactly replicated the shape of the mold (Figure 5G), which is attributed to the rearrangement of the crosslinked structures via dissociation and reassociation of active dynamic interactions facilitated by pressure or interfacial tension.[35] The characteristic endows the DICH with the capability of reprocessing, which can not only be shape-formed during the polymerization but also be redesigned through the remolding process.

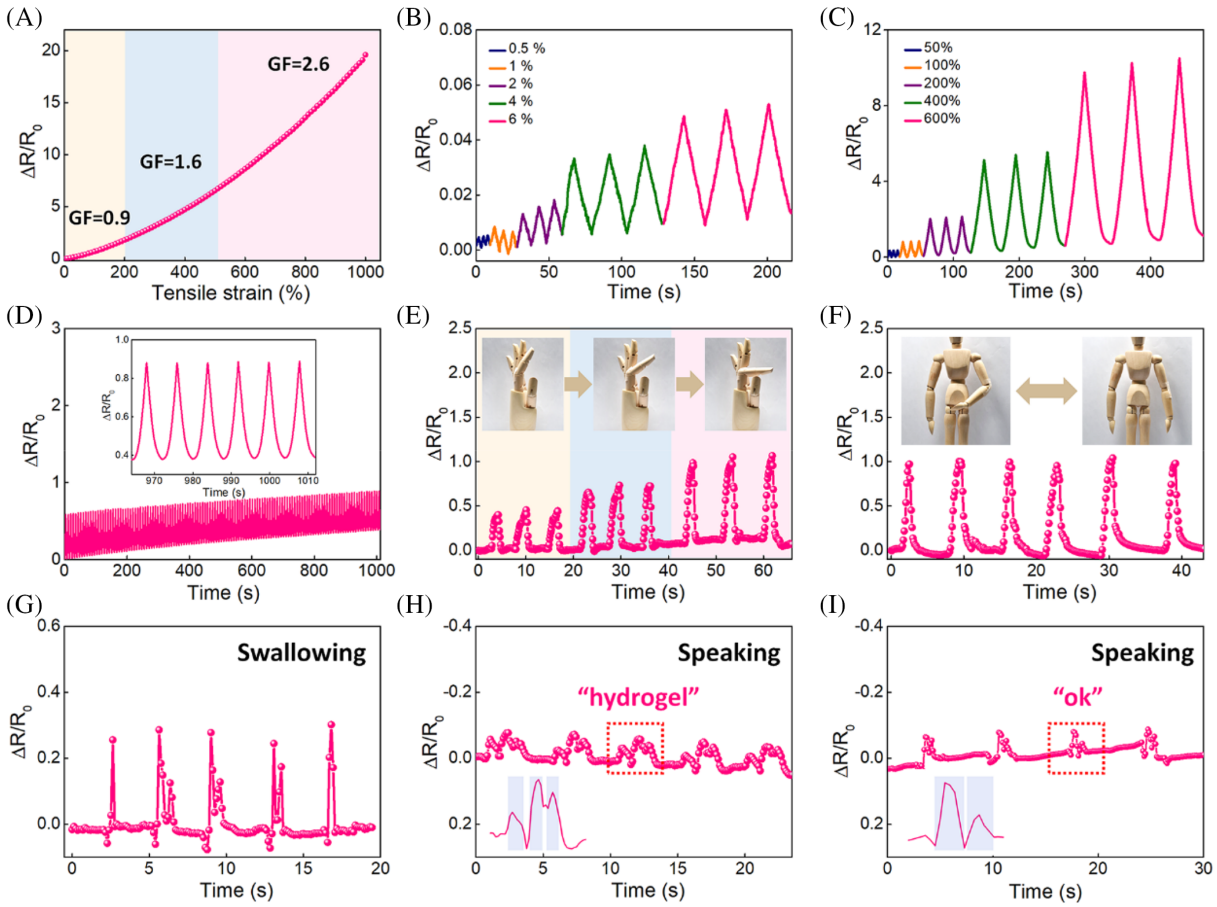

FIGURE 6 Strain sensing performance of DICHs. (A) Relative resistance variations as a function of tensile strain. Relative resistance variations under (B) small strains (0.5%, 1%, 2%, 4%, and 6%) and (C) large strains (50%, 100%, 200%, 400%, and 600%). (D) Cyclic stability tests under 50% strain for 100 cycles. Inset of (D) showing the enlarged areas. Relative resistance variations for real-time monitoring human movements of (E) finger bending, (F) elbow joint bending, (G) swallowing, pronouncing (H) "hydrogel" and (I) "OK"

Due to the substantial amounts of water and electrolytic ions, the DICH-2 shows a high ionic conductivity of 0.5 S m^{-1} measured from the EIS curve (Figure S13). Combined with the excellent stretchability, the DICH-2 is envisaged to be applied in stretchable ionic sensors to transduce deformations into electrical signals. The brightness of the LED connecting to an electric circuit gradually decreases as the strain increases, whereas it becomes bright as the stretching is slowly released (Figure S14), signifying that the conductivity of DICH-2 is strongly sensitive to various strains. During the tensile process, the ionic conductive path becomes narrower and the distance of the migration channel increases, thus increasing the resistance.[36]

The encapsulated DICH sensor was connected to a digital source meter to evaluate its strain sensing performance. The changes in resistance enhance sharply as mechanical strain increases (Figure 6A). To intuitively compare the *GF* values with those samples reported in the literature, the conventional method is piecewise fitting the $\Delta R/R_0$-ε curve.[37] A nonlinear segmental trend of $\Delta R/R_0$ is summarized as three linear segments per strain range: a *GF* of 0.9 for 0%–200%, a *GF* of 1.6 for 200%–500%, and a *GF* of 2.6 for the strain range of 500%–1000%, which are comparable to the reported hydrogel sensors (1.053–1.51).[38] The $\Delta R/R_0$ values increase gradually with increasing the strain from 0.5 to 600% (Figure 6B,C), which suggests its high sensitivity and reliability for sensing at both tiny and large strains. The response time in the stretching process is measured as 180 ms (Figure S15), implying the rapid response of the sensor. The sensors also show stable and repeated resistance changes with well-preserved amplitude after 100 continuous stretching-releasing cycles of 50% strain (Figure 6D). The resistance response of DICH to repeated stretching cycles is reversible without any attenuation, which indicates that the DICH-based sensor could be used for a long time due to its anti-fatigue properties.

To further demonstrate the practical applications of DICH in wearable ionic sensors, we tested the strain-induced sensitivity at the hydrogel-surface interface to monitor various human activities. After the sensor adheres to a wooden prosthetic finger (Figure 6E), the

bending of the finger to degrees of 30, 60, and 90° results in immediate increases in the relative resistance variations. Also, the resistance change signal has high repeatability and stability. Similarly, when sensors are connected to other joints of elbows and knees (Figures 6F and S16), the bending of joints can be detected sensitively and repeatedly. The sensors could also be used to identify tiny human movements. When the sensor is attached to the throat of a volunteer, the pressure caused by swallowing produces discernible changes in resistance (Figure 6G), which give incredible details of the throat movements. Compared with no signal changes produced by a microphone (Figure S17), when the tester pronounces the phrase "hydrogel" and "ok", the distinct and repeatable characteristic signals of time-dependent relative resistance variations are obtained (Figure 6H, I). These results demonstrate that the prepared DICH maintains stable mechanical and strain-sensitive performances.

To investigate the sensing capability after self-healing, the healed DICH sensor was used to characterize the sensing performance. Notably, the resistance change-strain curve of the healed hydrogel is similar to that of the corresponding original hydrogel (Figure S18a), implying that the healed DICH is still highly sensitive to the strain. Moreover, a self-healed DICH sensor is applied to monitor the bending motions of the elbow joint (Figure S18b). The signal intensity of the self-healed DICH sensor is similar to that of the initial one, indicating that the internal structure and ionic conductivity of the material are well recovered after self-healing. Moreover, cylindrical and self-healing cylindrical samples were pressed into a rectangular mold to characterize the sensing properties after reprocessing. The reprocessed DICH and its strain sensor still have excellent sensing capability and sufficient sensitivity to detect signals of elbow bending (Figures S19a,b and S20a,b). Based on this property, the DICHs could be made into various shapes according to the requirements of practical applications. In conclusion, compared with other ionic conductive hydrogels used in ionic sensors, the prepared DICH-based sensors have not only relatively high sensitivity and wide detection range but also critical performances of self-healing and reprocessing properties (Table S2). Based on the relations between relative resistance change and strain, the resultant DICH is promisingly applied to measure human motions.

3 | CONCLUSION

The DICH with the design of both hydrophobic association network and metal coordination network is one-pot fabricated. Owing to the presence of the dual dynamic networks, the fabricated DICH possesses a large stretchability of >2800%, moderate tensile/compressive strength of 270/960 kPa and high fracture toughness of 4820 kJ m^{-3}. The high reversibility of the dual dynamic networks enables the DICH with excellent notch insensitivity, reprocessing capability, and self-healability with a superior healing efficiency of >95%. The DICH sample, after being cut and self-healed, could withstand the further stretching over 18 times its original length. The DICH is further used as an ionic conductor to assemble a skin-inspired resistance strain sensor, demonstrating high sensitivity in a wide strain range. The sensor delivers a high sensitivity (*GF*: 2.6), low detection limit (as low as 0.5%), wide strain range (0.5%–600%), and short response time (180 ms). The DICH is also successfully applied as a wearable sensor to monitor various human motions, including large activities (e.g., finger, elbowing, knee bending) and tiny physiological signals (e.g., swallowing, speaking). Therefore, this study might explore the development of ultra-stretchable ionic conductive hydrogels with unique self-healability and reprocessibility, showing great prospects in the emerging adaptable and multifunctional skin-inspired ionic sensors.

ACKNOWLEDGMENT

This work was supported by the National Natural Science Foundation of China (52122303, 21875033).

ORCID

Chao Zhang https://orcid.org/0000-0003-1255-7183

REFERENCES

[1] (a) Z. Li, S. Zhang, Y. Chen, H. Ling, L. Zhao, G. Luo, X. Wang, M. C. Hartel, H. Liu, Y. Xue, R. Haghniaz, K. Lee, W. Sun, H. Kim, J. Lee, Y. Zhao, Y. Zhao, S. Emaminejad, S. Ahadian, N. Ashammakhi, M. R. Dokmeci, Z. Jiang, A. Khademhosseini, *Adv. Funct. Mater.* **2020**, *30*, 2003601. (b) H. Liu, H. Zhang, W. Han, H. Lin, R. Li, J. Zhu, W. Huang, *Adv. Mater.* **2021**, *33*, 2004782. (c) S.-N. Li, B. Li, Z.-R. Yu, S.-W. Dai, S.-C. Shen, M. Mao, L.-X. Gong, Y. Feng, D. Jia, Y. Zhou, L.-C. Tang, *ACS Appl. Polym. Mater.* **2020**, *2*, 1874. (d) L. Wang, G. Gao, Y. Zhou, T. Xu, J. Chen, R. Wang, R. Zhang, J. Fu, *ACS Appl. Mater. Interfaces* **2019**, *11*, 3506.

[2] (a) X. Di, J. Li, M. Yang, Q. Zhao, G. Wu, P. Sun, *J. Mater. Chem. A* **2021**, *9*, 20703. (b) Q. Yu, Z. Qin, F. Ji, S. Chen, S. Luo, M. Yao, X. Wu, W. Liu, X. Sun, H. Zhang, Y. Zhao, F. Yao, J. Li, *Chem. Eng. J.* **2021**, *404*, 126559. (c) Y. M. Kim, H. C. Moon, *Adv. Funct. Mater.* **2020**, *30*, 1907290.

[3] X. Pei, H. Zhang, Y. Zhou, L. Zhou, J. Fu, *Mater. Horiz.* **1872**, *2020*, 7.

[4] (a) M. Zhang, J. Yu, K. Shen, R. Wang, J. Du, X. Zhao, Y. Yang, K. Xu, Q. Zhang, Y. Zhang, Y. Cheng, *Chem. Mater.* **2021**, *33*, 6453. (b) B. Cheng, Y. Li, H. Li, H. Li, S. Yang, P. Li, Y. Shang, *Compos. Sci. Technol.* **2021**, *213*, 108948.

[5] (a) Y. Ye, Y. Zhang, Y. Chen, X. Han, F. Jiang, *Adv. Funct. Mater.* **2020**, *30*, 2003430. (b) Z. Wang, J. Chen, L. Wang, G. Gao, Y. Zhou, R. Wang, T. Xu, J. Yin, J. Fu, *J. Mater. Chem. B* **2019**, *7*, 24.
[6] (a) H. Huang, L. Han, X. Fu, Y. Wang, Z. Yang, L. Pan, M. Xu, *Adv. Electron. Mater.* **2020**, *6*, 2000239. (b) G. Gao, F. Yang, F. Zhou, J. He, W. Lu, P. Xiao, H. Yan, C. Pan, T. Chen, Z. L. Wang, *Adv. Mater.* **2020**, *32*, 2004290. (c) X. Li, L. He, Y. Li, M. Chao, M. Li, P. Wan, L. Zhang, *ACS Nano* **2021**, *15*, 7765.
[7] Q. Chen, L. Zhu, C. Zhao, Q. Wang, J. Zheng, *Adv. Mater.* **2013**, *25*, 4171.
[8] D. Kim, S.-K. Ahn, J. Yoon, *Adv. Mater.* **2019**, *4*, 1800739.
[9] C. Liu, N. Morimoto, L. Jiang, S. Kawahara, T. Noritomi, H. Yokoyama, K. Mayumi, K. Ito, *Science* **2021**, *372*, 1078.
[10] S. Xia, Q. Zhang, S. Song, L. Duan, G. Gao, *Chem. Mater.* **2019**, *31*, 9522.
[11] S. Das, P. Martin, G. Vasilyev, R. Nandi, N. Amdursky, E. Zussman, *Macromolecules* **2020**, *53*, 11130.
[12] X. Li, Y. Wang, D. Li, M. Shu, L. Shang, M. Xia, Y. Huang, *Soft Matter* **2021**, *17*, 6688.
[13] G. Jiang, C. Liu, X. Liu, G. Zhang, M. Yang, F. Liu, *Macromol. Mater. Eng.* **2009**, *294*, 815.
[14] J. Huang, Y. Liu, X. Chi, Y. Jiang, Z. Xu, G. Qu, Y. Zhao, Z. Li, C. Chen, G. Chen, X. Wu, J. Ren, *J. Mater. Chem. A* **2021**, *9*, 963.
[15] Z. Liu, P. Yao, *RSC Adv.* **2015**, *5*, 103292.
[16] N. Yuan, L. Xu, H. Wang, Y. Fu, Z. Zhang, L. Liu, C. Wang, J. Zhao, J. Rong, ACS. Appl, *Mater. Interfaces* **2016**, *8*, 34034.
[17] M. Kang, O. Oderinde, S. Liu, Q. Huang, W. Ma, F. Yao, G. Fu, *Carbohydr. Polym.* **2019**, *203*, 139.
[18] T. Zhu, Q. Feng, S. Liu, C. Zhang, *Compos. Commun.* **2020**, *20*, 100376.
[19] (a) Y. Zheng, H. Song, S. Chen, X. Yu, J. Zhu, J. Xu, K. A. I. Zhang, C. Zhang, T. Liu, *Small* **2020**, *16*, 2004342. (b) Y. Zheng, S. Chen, K. A. I. Zhang, J. Zhu, J. Xu, C. Zhang, T. Liu, *ACS Appl. Mater. Interfaces* **2021**, *13*, 13328.
[20] (a) X. Wang, Y. Wang, H. Hou, J. Wang, C. Hao, ACS. Sustain, *Chem. Eng.* **2017**, *5*, 6438. (b) H. Song, Y. Sun, J. Zhu, J. Xu, C. Zhang, T. Liu, *Compos. Part B-Eng.* **2021**, *217*, 108901.
[21] (a) Y. Wang, Y. Liu, R. Plamthottam, M. Tebyetekerwa, J. Xu, J. Zhu, C. Zhang, T. Liu, *Macromolecules* **2021**, *54*, 3832. (b) P. Shi, Y. Wang, K. Wan, C. Zhang, T. Liu, *Adv. Funct. Mater.* **2022**, *32*, 2112293.
[22] L. Li, Y. Zhang, H. Lu, Y. Wang, J. Xu, J. Zhu, C. Zhang, T. Liu, *Nat. Commun.* **2020**, *11*, 62.
[23] A. Wang, Y. Wang, B. Zhang, K. Wan, J. Zhu, J. Xu, C. Zhang, T. Liu, *Chem. Eng. J.* **2021**, *411*, 128506.
[24] W. Sun, B. Xue, Q. Fan, R. Tao, C. Wang, X. Wang, Y. Li, M. Qin, W. Wang, B. Chen, Y. Cao, *Sci. Adv.* **2020**, *6*, eaaz9531.
[25] (a) J. P. Gong, Y. Katsuyama, T. Kurokawa, Y. Osada, *Adv. Mater.* **2003**, *15*, 1155. (b) X. Xu, V. V. Jerca, R. Hoogenboom, *Mater. Horiz.* **2021**, *8*, 1173.
[26] (a) J. Yang, Y. Du, X. Li, C. Qiao, H. Jiang, J. Zheng, C. Lin, L. Liu, *ChemPlusChem* **2020**, *85*, 2158. (b) F. Mo, Z. Wang, R. Jiang, W. Gai, Q. Li, S. Lv, C. Zhi, *Sci. China Mater.* **2021**, *64*, 2764.
[27] F. Wang, Z. Yang, J. Li, C. Zhang, P. Sun, *ACS Macro Lett.* **2021**, *10*, 510.
[28] (a) H. Wang, L. Dai, D. Chai, Y. Ding, H. Zhang, J. Tang, *J. Colloid Interf. Sci.* **2020**, *561*, 629. (b) H. Chen, B. Hao, P. Ge, S. Chen, *Polym. Chem.* **2020**, *11*, 4741. (c) Y. Guo, X. Zhou, Q. Tang, H. Bao, G. Wang, P. Saha, *J. Mater. Chem. A* **2016**, *4*, 8769. (d) R. Li, T. Fan, G. Chen, H. Xie, B. Su, M. He, *Chem. Eng. J.* **2020**, *393*, 124685. (e) X. Yu, Y. Zheng, H. Zhang, Y. Wang, X. Fan, T. Liu, *Chem. Mater.* **2021**, *33*, 6146.
[29] B. Zhang, X. Zhang, K. Wan, J. Zhu, J. Xu, C. Zhang, T. Liu, *Research* **2021**, *2021*, 9761625.
[30] J. Mao, C. Zhao, Y. Li, D. Xiang, Z. Wang, *Compos. Commun.* **2020**, *17*, 22.
[31] K. Xu, Y. Wang, B. Zhang, C. Zhang, T. Liu, *Compos. Commun.* **2021**, *24*, 100677.
[32] K. Cui, Y. N. Ye, C. Yu, X. Li, T. Kurokawa, J. P. Gong, *ACS Macro Lett.* **2020**, *9*, 1582.
[33] M. He, H. Zhang, W. Chen, X. Dong, *Polymer Physics, Fudan University Press, Shanghai*, P. R. China **2008**, Fudan University Press.
[34] K. Li, X. Zan, C. Tang, Z. Liu, J. Fan, G. Qin, J. Yang, W. Cui, L. Zhu, Q. Chen, *Adv. Sci.* **2022**, *9*, 2105742.
[35] G. Jiang, C. Liu, X. Liu, Q. Chen, G. Zhang, M. Yang, F. Liu, *Polymer* **2010**, *51*, 1507.
[36] Y. Gao, Y. Wang, S. Xia, G. Gao, *Sci. China Mater.* **2021**, *64*, 2313.
[37] Z. Wang, H. Zhou, D. Liu, X. Chen, D. Wang, S. Dai, F. Chen, B. Xu, Adv. *Funct. Mater.* **2022**, *32*, 2201396.
[38] (a) H. Sun, Y. Zhao, C. Wang, K. Zhou, C. Yan, G. Zheng, J. Huang, K. Dai, C. Liu, C. Shen, *Nano Energy* **2020**, *76*, 105035. (b) Y. Chen, J. Zhu, H.-Y. Yu, Y. Li, *Compos. Sci. Technol.* **2020**, *194*, 108165.

SUPPORTING INFORMATION

Additional supporting information can be found online in the Supporting Information section at the end of this article.

How to cite this article: H. Song, B. Zhang, Q. Feng, D. H. Nguyen, C. Zhang, T. Liu, *J. Polym. Sci.* **2022**, *60*(19), 2817. https://doi.org/10.1002/pol.20220266